

Theory and Measurements of the Transverse Wake Due to Beamline Collimators.

Stephen Molloy,* Ray Arnold, Doug McCormick, Zen Szalata, and Mike Woods
*Stanford Linear Accelerator Center,
 Menlo Park, CA94025, USA.*

Nigel Watson
*STFC/RAL/ASTeC,
 Chilton, Didcot, UK.*

Carl Beard and Juan Luis Fernandez-Hernando
*Daresbury Laboratory,
 Warrington, UK.*

Adriana Bungau
*University of Manchester,
 Manchester, UK.*

Jonathon Smith and Andre Sopczak
*University of Lancaster,
 Lancaster, UK.*

(Dated: October 30, 2008)

This is just a place-holder abstract copied from a previous paper. Don't take it seriously! We report on measurements of the transverse wakefields induced by collimators of differing characteristics. An apparatus allowing the insertion of different collimator jaws into the path of a beam was installed in End Station A (ESA) in SLAC. Eight comparable collimator geometries were designed, including one that would allow easy comparison with previous results, and were installed in this apparatus. Measurements of the beam kick due to the collimator wakefields were made with a beam energy of 28.5 GeV, and beam dimensions of 100 microns vertically and a range of 0.5 to 1.5 mm longitudinally. The trajectory of the beam upstream and downstream of the collimator test apparatus was determined from the outputs of ten BPMs (four upstream and six downstream), thus allowing a measurement of the angular kick imparted to the beam by the collimator under test. The transverse wakefield was inferred from the measured kick. The different aperture designs, data collection and analysis, and initial comparison to theoretical and analytic predictions are presented here.

PACS numbers: Valid PACS appear here

I. INTRODUCTION

At the International Linear Collider (ILC) [1] it is expected that significant beam halo will be generated in the acceleration and final focus regions. Allowing this charge to traverse the interaction region (IR) will yield negligible luminosity increase, but, if scattered into the detector by the strong fields of the colliding beams, will degrade its resolution, and, possibly, cause damage. For this reason a collimation section is included in the design of the beam delivery system.

The design for this section involves restricting the aperture of the beampipe at various locations in order to halt any particles located far from the core of the bunch. Correct longitudinal positioning of these inserts will lead to the halo being removed for all betatron phases.

As well as continuously absorbing a fraction of the

power of the beam, the collimators must be designed to withstand a impact by an entire bunch. Typically a long ($> 20\chi_0$) collimator is "shadowed" by a short ($0.6 - 1.0\chi_0$) spoiler, whose purpose is to enlarge the size of the beam through multiple Coulomb scattering prior to absorption by the collimator, thus reducing the incident power density and the likelihood of damage.

It is well known that the electro-magnetic field of a charged bunch propagating through a metallic beam-pipe with a relativistic velocity may be disrupted by changes in the geometry of the cross-section of that pipe, and that this disruption may be exacerbated by the finite resistivity of the beam pipe wall [2]. In certain situations, the fields excited by the head of the bunch may act on the tail, inducing emittance growth, or, in the worst case, break-up of the beam. These fields are typically referred to as "wakefields".

Since each of the collimators provide a change in the cross-section of the beam-pipe, it is expected that they will generate wakefields, and are therefore an area of potential emittance growth. For this reason it is important

*Electronic address: smolloy@slac.stanford.edu

TABLE I: Specifications of the ESA beam.

Beam Property	Value
Charge	$1 - 2 \times 10^{10} e^-$
Energy	28.5 GeV
Rep. rate	10 Hz
Bunch length	0.3 - 1.0 mm
Bunch height \times width	100 μm \times 1 mm

to design collimators to minimise the wakefields they will generate, and, therefore, their impact on the beam.

Although previous studies [3] have advanced the ability of modelling codes to predict the measured data to within a factor of $\sim 2 - 3$, they have also demonstrated that performing analytical calculations of these fields can be prohibitively complex, even in very simplified cases.

In order to design suitable collimators for the ILC, a goal has been set of a $\sim 10\%$ agreement between the measured and predicted transverse wakes. This paper discusses an experiment to measure the transverse wake generated by a range of different collimators, and to show the level of agreement of these measurements with theoretical and simulated results.

II. THEORY

Something about the theory here, including the different geometric regimes, the resistive wall kick, the validity of the equations, and the expected accuracy of their results.

III. DESCRIPTION OF EXPERIMENT

Experimental measurements of the collimator kicks were performed at the End Station A (ESA) facility [4] at the Stanford Linear Accelerator Center (SLAC). The basic idea behind the experiment is to excite transverse wakefields by passing a bunch of electrons through a collimator at various offsets from its centre, and deduce the scale of the wakefield from the transverse kick received by the bunch.

The ESA facility uses an electron beam extracted from the SLAC linac after acceleration to 28.5 GeV, and steered around a 24.5° bend. There are no magnetic elements in the experimental region of ESA, with the exception of a dipole chicane used in a spectrometry experiment. Table I shows the properties of the ESA beam.

Performing this experiment at ESA yields several advantages:

1. Since ESA is a facility dedicated to ILC beam-tests, experimenters have control over its operation during their shifts. This means that frequent accesses are possible, and the experimenters have full control over the beam conditions.

2. The long bend immediately upstream of ESA allows control over the bunch length in ESA via the phase of the accelerating RF in the linac. See table I.

3. ESA is equipped with several cranes that facilitate installation of the measurement apparatus (described in subsection III A).

Upstream of the collimator experiment were four RF cavity beam position monitors (BPMs). These were arranged as two doublets; one 44.5 m and one 4 m from the collimator teststand. Downstream were two triplets of BPMs; one 13 m away, and the other 29 m. The trajectory reconstructed from these measurements was used to calculate the kick received from the collimator wakefield.

With an estimated $1 \mu\text{m}$ uncorrelated, RMS, error on the position measurement from each BPM, the theoretical measurement accuracy of the kick measurement is ~ 40 n-rad. As the downstream BPMs were part of an evolving R&D project, their arrangement was altered for some of the run periods referred to in this paper. The changes, however, were simple rearrangements of the BPMs, as well as the addition of an extra BPM, thus having negligible impact on the theoretical resolution of the wakefield kick measurement.

A. Collimator Wakefield Apparatus

A so-called “wakefield box” was installed in ESA for the purpose of testing various collimators. This apparatus is detailed in [5], and a schematic is shown in figure 1.

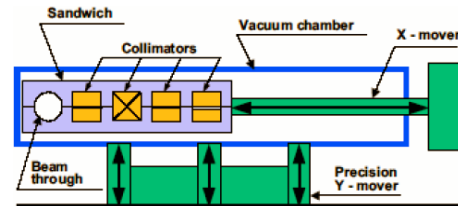


FIG. 1: Schematic of the wakefield collimator box.

As shown in figure 1, the wakefield box contains an inner “sandwich” in which the collimators to be tested are installed. There are five possible slots through which the beam can move, and four of these are machined to allow installation of collimator jaws. The fifth is left free of obstruction to allow other ESA experiments to run without interruption. An “X-mover” is used to move the box to change the slot presented to the beam.

The sandwich is contained within a vacuum chamber, which rests on three motor controlled cams as shown in figure 2. This system of motors allows control of the wakefield box in y , z , and dy/dz , where y is the vertical axis, and z is in the direction of beam motion. Full details, including equations of motion, can be found in [6]. For the purposes of this paper it is important to note that

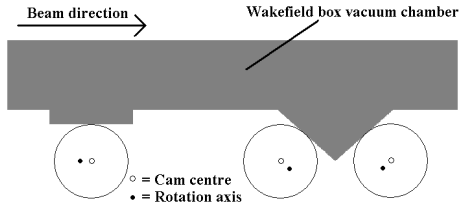


FIG. 2: Cartoon of the cam mover system used to control the wakefield box.

this system allows the wakefield box to move ± 1.4 mm vertically, and that motion in one degree of freedom will reduce the achievable range in the other two. LVDT sensors with a specified resolution of the order of $1 \mu\text{m}$ were installed at various points on the wakefield box vacuum chamber to provide a readback to the mover control software.

The measurement can proceed by maintaining a steady beam trajectory with position and energy feedbacks, whilst moving the collimator vertically with respect to the beam. This provides more accurate knowledge of the relative offset, and, therefore, the scaling of the wakefield kick with the beam position.

B. Collimators Tested

The collimators tested in ESA are illustrated in figures 3, 4, 5, and 6. Shown in these figures are the side and beam view of each of the designs, as well as specifications for the half-gap (that is, the distance from the midpoint of the aperture to one of the collimator edges), and the angle of the taper. The differing colours of the sketches in figure 5 distinguish different materials and surface finishes, the details of which are covered in the following text.

Collim. #	Side view	Beam view	Revised 4-May-2006
1	α $r=1/2 \text{ gap}$	$h=38 \text{ mm}$ $h=38 \text{ mm}$	$\alpha=324\text{mrad}$ $r=2.0\text{mm}$
2			$\alpha=324\text{mrad}$ $r=1.4\text{mm}$
3	$L=1000 \text{ mm}$		$\alpha=324\text{mrad}$ $r=1.4\text{mm}$
4	7 mm		$\alpha=\pi/2\text{rad}$ $r=4.0\text{mm}$

FIG. 3: Schematic of the collimators from sandwich 1.

The justifications for each of the collimator choices are as follows;

Collim.#	Side view	Beam view	Revised 4-May-2006
8	133 mm	38 mm $h=38 \text{ mm}$	$r_1=4.0\text{mm}$ $r_2=1.4\text{mm}$ $\alpha_1=289\text{mrad}$ $\alpha_2=166\text{mrad}$
7	31 mm		$\alpha_1=\pi/2 \text{ rad}$ $\alpha_2=166\text{mrad}$ $r_1=4.0\text{mm}$ $r_2=1.4\text{mm}$
6	211 mm		$\alpha=166\text{mrad}$ $r=1.4\text{mm}$
5	7 mm		$\alpha=\pi/2\text{rad}$ $r=1.4\text{mm}$

FIG. 4: Schematic of the collimators from sandwich 2.

Collim.#	Side view	Beam view	Revised 27-Nov-2006
6	$\sim 211 \text{ mm}$ 1.4 mm α	38 mm $h=38 \text{ mm}$	$\alpha=166\text{mrad}$ $r=1.4\text{mm}$ (1/2 gap)
10	$\sim 21 \text{ mm}$ α		$\alpha=166\text{mrad}$ $r=1.4\text{mm}$
11	$\sim 21 \text{ mm}$ α		$\alpha=166\text{mrad}$ $r=1.4\text{mm}$
12	$\sim 21 \text{ mm}$ α		$\alpha=166\text{mrad}$ $r=1.4\text{mm}$

FIG. 5: Schematic of the collimators from sandwich 3.

- Collimator 1

This geometry is identical to one tested in a previous measurement [3], and was included in these tests in order to control systematic errors.

- Collimator 2

Identical to collimator 1, but with a smaller half gap. Investigates the kick factor's dependence on the half gap.

- Collimator 3

Identical half gap and taper angle to collimator 2, but with a long flat section, intended to add a large resistive component to the kick.

- Collimator 4

Purely diffractive step of 0.5 radiation length thickness. Allows direct comparison with collimator 5, measuring half-gap dependence.

- Collimator 5

Collim.#	Side view	Beam view	Revised 27-Nov-2006
13	OFE Cu α_2 =21 mm ~52 mm	38mm h=38 mm	$\alpha_1=\pi/2$ rad $\alpha_2=166$ mrad $r_1=4.0$ mm $r_2=1.4$ mm
14	Ti6Al4V α_2 =21 mm ~52 mm		$\alpha_1=\pi/2$ rad $\alpha_2=166$ mrad $r_1=4.0$ mm $r_2=1.4$ mm
15	α_2 =21 mm ~125 mm		$\alpha_1=\pi/2$ rad $\alpha_2=50$ mrad $r_1=4.0$ mm $r_2=1.4$ mm
16	OFE Cu =21 mm		non-linear taper $r=1.4$ mm

FIG. 6: Schematic of the collimators from sandwich 4.

Purely diffractive step of 0.5 radiation length thickness. Allows direct comparison with collimator 4, measuring half-gap dependence.

- Collimator 6

Same half-gap as collimators 2 and 5, but with significantly shallower taper angle. Note that this collimator is repeated in figure 5.

- Collimator 7

For comparison with collimator 4 ($\pi/2$ taper angle to a half gap of 4 mm), and collimator 6 (identical taper angle at the minimum aperture).

- Collimator 8

For comparison with collimators 6 and 7.

- Collimator 10

A roughened copper version of collimators 11 and 12 for the purpose of testing the dependence on surface roughness.

- Collimator 11

Constructed from a titanium alloy (Ti6Al4V), this can be compared to collimators 10 and 12 to determine the dependence on the resistivity of the collimator material.

- Collimator 12

Equivalent in shape to collimators 10 and 11, this allows comparison of the effect of the surface finish, and bulk material.

- Collimator 13

Same taper angle and flat section as collimators 10, 11, and 12, but with an initial $\pi/2$ step, to further investigate the effect of a sharp change of geometry.

- Collimator 14

Identical geometrically to collimator 13, but constructed from the same titanium alloy as collimator 11.

- Collimator 15

Similar to collimator 13, but with a shallower secondary taper.

- Collimator 16

Something about impedance matching and cosine curves...

IV. SIMULATIONS

A. Choice of Codes for the Solution of Collimator Wakefield Kicks

Over the last three years there have been significant advances in the tools available for calculation of collimator kicks in three spatial dimensions. In 2006[C. Beard & J. Smith EPAC'06] we reported on the use of MAFIA for solving such problems, and while this was somewhat effective for short step collimators, it was clear that a standard desktop PC was unable to solve these problems in 3D. We will report on the validity of the quasi-2D approximation, which is a powerful tool for optimisation and estimations before more detailed calculations are required. The previous 'state of the art' for collimator calculations is described by Ng[Numerical Calculations of Short-Range Wakes of Collimators, PAC2001]

It was clear that if we used standard finite difference time domain methods we would find ourselves with problems of a size only large clusters and supercomputers could handle. Thankfully, a number of codes have appeared that implement 'moving mesh' algorithms. Amongst those are the code we used for the greater part of our study, GdfidL. Moving mesh, or 'window wake' calculations are also possible with PBCI and ECHO. Both PBCI and ECHO feature algorithms to make the calculations non-dispersive, which reduces numerical noise in the results. Moderately short bunches can also be calculated with recent versions CST particle studio, however without a window wake or parallel running it suffers the same problems as MAFIA, and cannot yet handle short bunch lengths. We will report on those results too. Tau 3P, VORPAL, MEEP and NEKCEM also do not have a moving mesh, and while parallel calculations can be performed with these codes too, it is thought that ECHO, GdfidL and PBCI are currently the most appropriate for this type of calculation. CST Particle Studio claims to handle resistive wall wakes in the same calculations. We restrict ourselves to geometric wake only calculations, leaving the inclusion of resistive effects in numerical codes as future work.

B. T480 Calculations

At the T480 experiment at SLAC the collimators had twelve distinct geometries. Calculations of the transverse loss as well as kick factor were produced at a variety of different offsets in order to understand the higher order mode dependence. While the collimators are designed to understand ILC requirements with a bunch length of 0.3 mm, we have chosen to concentrate largely on 0.5 mm and 1 mm bunch lengths, as these correspond more closely with the ESA beam available at SLAC. For each collimator, bunch length, and offset a resolution convergence was performed, using a procedure described separately by the authors allowing an estimate of uncertainty to be made [some EUROTeV memo - may also include choices for turning transverse loss factor at various offsets into trans kick]. The results from these calculations are shown in table II.

example plot of analytic transverse wake potential, GdfidL wake, PBCI wake

For each of 12 geometries show Experimental, GdfidL 500/1000 results overlapping? I think these images

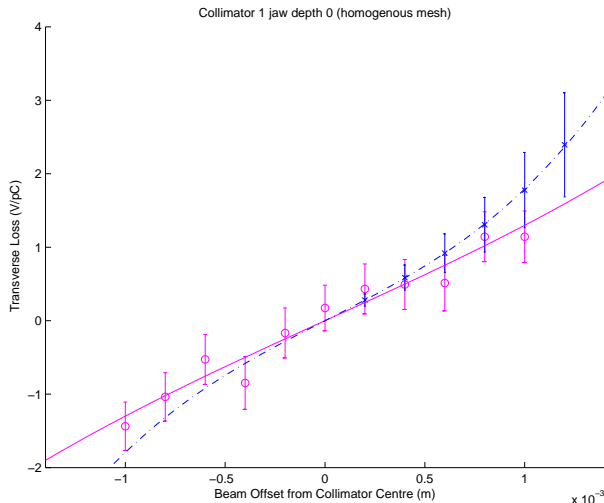


FIG. 7: Experimental and calculated loss factors for collimator 1.

would be better combined into a single figure. Maybe we should include plots for all 12 geometries, or all 16 collimators. Discuss... We can see that in many cases the loss factor calculated in GdfidL bares close resemblance to that observed in experiment, however the calculated value contains neither resistive or surface wall wake effects, and there remains uncertainty in bunch length. (reference George & Victoria's paper if it's out in time?)

Explain which results show good agreement, explanation for those that don't. ** Placeholder with existing results from Old GdfidL?? Expected accuracy

Discuss future work on entire assembly?

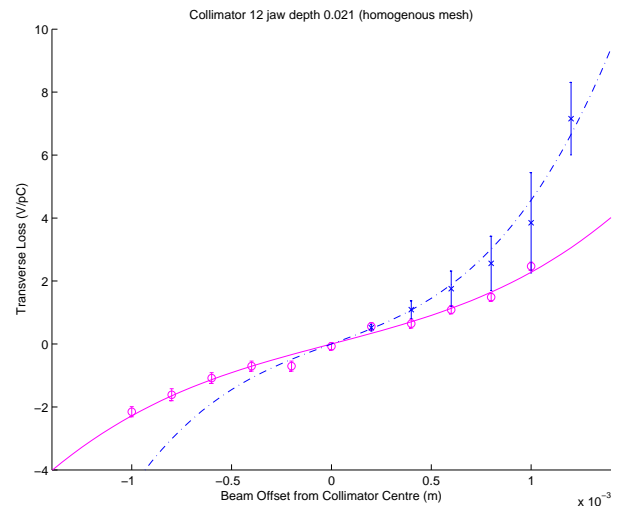


FIG. 8: Experimental and calculated loss factors for collimator 12.

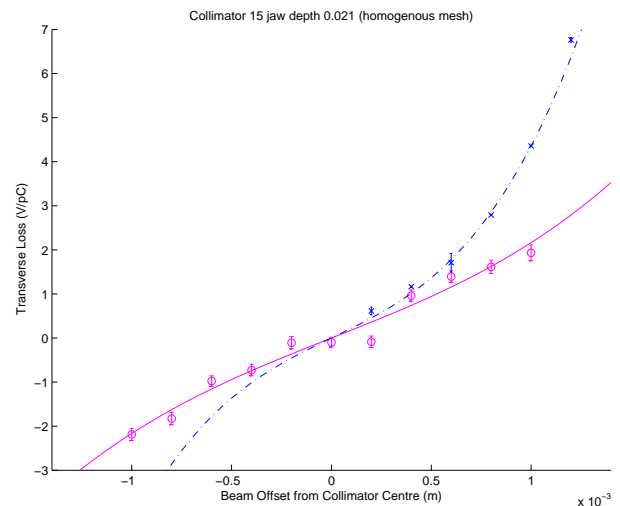


FIG. 9: Experimental and calculated loss factors for collimator 15.

V. MEASUREMENTS

These collimators were measured over a series of run periods that extended over approximately two years. Due to the large time period between each of these runs, there was a danger of systematic differences in the experiment biasing the results. In order to defend against this possibility, the selection of collimators tested during each run period included at least one that had been measured previously, causing systematic differences to be readily apparent.

As shown in figure 1, it was possible to install four collimators on the beamline for testing. A typical shift would involve presenting each collimator in turn to the beam, and causing the beam to pass through the collimator jaws at a range of vertical positions. This would be repeated

TABLE II: Calculated Transverse Geometric Kick Factors for ESA T480 Collimators

Collimator	Analytic (Geometric only)	GdfidL (0.5 mm)	GdfidL (1 mm)	ECHO 3D (0.5 mm)	PBCI (0.5 mm)
1	2.246	1.39 ± 0.29		1.7	
2	5.894	3.06 ± 0.02		3.1	
3	5.894	$5.57 \pm$		5.1	
4	0.561	$0.78 \pm$		0.77	
5	4.584	$6.07 \pm$		6.8	
6,9	4.219	$1.64 \pm$		2.3	
7	4.244*	$2.80 \pm$		2.7	
8	4.219*	$2.62 \pm$		2.4	
10,11,12	4.219	\pm			
13,14	4.219*	\pm			
15	4.219*	\pm			
16		\pm			

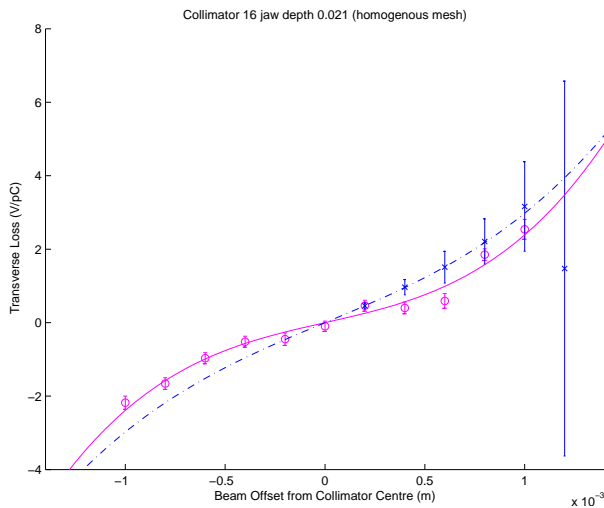


FIG. 10: Experimental and calculated loss factors for collimator 16.

several times with the nominal beam parameters in order to gather statistics, and also at multiple bunch lengths and charges in order to confirm the expected scaling with these parameters.

The transverse position of the beam was controlled by a feedback, however there was expected to be a scale error between the step sizes given to the position feedbacks and the actual step of the beam position. Vertical stepper motors on the wakefield box (described in section III A) were expected to be significantly more accurate than the beam feedbacks, so it was decided to hold the beam in the centre of the jaws using these feedbacks, and move the collimators around it.

First the beam feedbacks were tweaked in order to place the beam at the approximate centre of the collimator jaws. To do this, the jaws were scanned in both directions in order to find the point at which significant beam scraping occurred. The feedbacks were then adjusted in such a way that the range of motion upwards was approximately equal to the downward range. This method found the centre with an accuracy of $\sim 100 \mu\text{m}$

(roughly the vertical size of the bunch).

How the measurements were done. Different charges, and bunch lengths.....

VI. DATA ANALYSIS

A. Bunch Length

As detailed in section IV, the wakefield kick is sensitive to the length of the bunch, so it is important that this be controlled and quantified for each of the measurements. The techniques used to measure the bunch length in ESA is detailed in [7], and will be described here briefly.

Due to a lack of suitable diagnostics in ESA it was not possible to perform a direct measurement of this quantity, however since the transfer matrix of the bend is well known, a measurement of the longitudinal phase space of the beam as it enters the bend allows a prediction of the longitudinal phase space in ESA, and, therefore, the expected bunch length.

A screen was used to record an image of the synchrotron radiation emitted by the beam as it moved around the bend. Due to the non-zero dispersion in this region of the machine, the horizontal distribution of this image gives the energy distribution of the bunch.

A transverse cavity at the end of the linac was phased so that the zero crossing of the rf coincided with the longitudinal centre of the bunch. This results in the electrons being given a transverse (vertical) kick, whose amplitude is, to first order, proportional to their longitudinal position within the bunch.

Thus the synchrotron light image contains an expansion of both longitudinal coordinates, and, after calibration of this system, allows extraction of an image of the longitudinal phase space (see figure 11).

$$z_2 = z_1 + R_{56} \cdot \frac{dE}{E} \quad (1)$$

Given the measured profile and the R -matrix of the bend, it was possible to calculate the expected longitu-

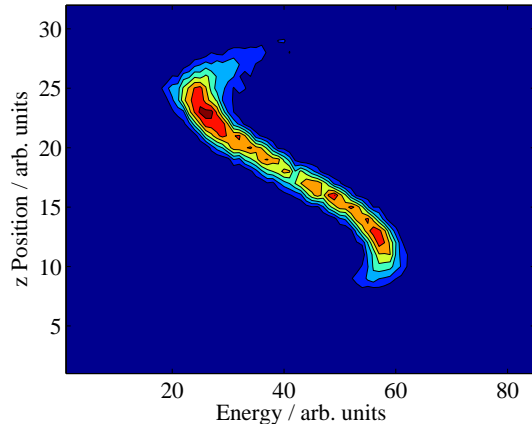


FIG. 11: A digitisation of the synchrotron light image formed at a high dispersion point of the A-line, and with a transverse cavity kicking the beam vertically.

dinal profile in ESA using equation 1, where z_i is the longitudinal position of each particle ($i = 1$ indicates the bunch before the bend, $i = 2$ indicates the bunch after the bend), R_{56} is the (5, 6) term of the R -matrix, E is the design energy of the bunch, and dE is the energy error for each particle.

By varying the phase of the accelerating rf in the linac it was possible to obtain a wide range of bunch lengths in ESA (see table I).

Due to the destructive nature of this measurement it was not possible to use it as a continuous measurement of the bunch length. Instead high frequency diodes and a pyro-detector were installed in ESA for this purpose.

These devices are also described in [7]. The basic principle is that a beam will radiate energy if it passes a ceramic gap in the beamline, and the spectrum of this radiation will be a close approximation to the longitudinal profile of the bunch. Therefore, if the radiation is monitored in a frequency band whose wavelength is comparable to the length of the bunch, then any variation in this quantity can be measured. These devices were calibrated

against the length extracted from the synchrotron light measurement, and thus provided a non-invasive monitor of the bunch length in ESA.

Should probably estimate errors on this measurement, but it's been so long..... I have some data-archaeology to do!

B. Wakefield Kicks

How we extracted the kick factor from the data. Different types of fit. Combining data.

VII. RESULTS

Theoretical, simulated, and measured results.

Demonstration of consistency of measured results between different data-sets (including PT's). Results from combination of data-sets.

VIII. DISCUSSION

Discuss the results and do comparison with theory and simulation.

IX. CONCLUSIONS

Some conclusions. Identify further work.

Acknowledgments

We wish to acknowledge the support of the operations staff at SLAC, and,

APPENDIX A: APPENDIX

-
- [1] J. Brau et al. (2007), iLC-REPORT-2007-001.
 - [2] W. K. H. Panofsky and M. Bander, *Rev. Sci. Instrum.* **39**, 206 (1968).
 - [3] P. Tenenbaum et al., *Phys. Rev. ST Accel. Beams* **10**, 034401 (2007).
 - [4] M. Woods et al. (2005), physics/0505171.
 - [5] P. Tenenbaum et al. (1999), contributed to IEEE Particle

- Accelerator Conference (PAC 99), New York, NY, 29 Mar - 2 Apr 1999.
- [6] G. Bowden, P. Holik, S. R. Wagner, G. Heimlinger, and R. Settles, *Nucl. Instrum. Meth.* **A368**, 579 (1996).
- [7] S. Molloy et al., PAC (07), contributed to Particle Accelerator Conference, Albuquerque, New Mexico, 25-29 Jun 2007.